INFECTION AND IMMUNITY, Mar. 2007, p. 1116–1128 Vol. 75, No. 3
0019-9567/07/$08.00+0 doi:10.1128/IAI.00902-06

Functional Characterization of the *Plasmodium falciparum* and *P. berghei* Homologues of Macrophage Migration Inhibitory Factor▽

Kevin D. Augustijn,[1] Robert Kleemann,[2] Joanne Thompson,[3] Teake Kooistra,[2] Carina E. Crawford,[3] Sarah E. Reece,[3] Arnab Pain,[4] Arjan H. G. Siebum,[5] Chris J. Janse,[1] and Andrew P Waters[1]*

Department of Parasitology, LUMC, Albinusdreef 2, 2333 ZA, Leiden, The Netherlands[1]; Vascular and Metabolic Diseases, TNO-Quality of Life, Zernikedreef 9, 2333 CK, Leiden, The Netherlands[2]; Institute of Immunology and Infection Research, Kings Buildings, Ashworth Laboratories, West Mains Road, EH9 3JT Edinburgh, United Kingdom[3]; The Wellcome Trust Sanger Institute, Hinxton, CB10 1SA Cambridge, Cambridge, United Kingdom[4]; and Leiden Institute of Chemistry, Gorlaeus Laboratories, Einsteinweg 55, 2333 CC, Leiden, The Netherlands[5]

Received 7 June 2006/Returned for modification 16 August 2006/Accepted 3 December 2006

Macrophage migration inhibitory factor (MIF) is a mammalian cytokine that participates in innate and adaptive immune responses. Homologues of mammalian MIF have been discovered in parasite species infecting mammalian hosts (nematodes and malaria parasites), which suggests that the parasites express MIF to modulate the host immune response upon infection. Here we report the first biochemical and genetic characterization of a *Plasmodium* MIF (*P*MIF). Like human MIF, histidine-tagged purified recombinant *P*MIF shows tautomerase and oxidoreductase activities (although the activities are reduced compared to those of histidine-tagged human MIF) and efficiently inhibits AP-1 activity in human embryonic kidney cells. Furthermore, we found that *Plasmodium berghei* MIF is expressed in both a mammalian host and a mosquito vector and that, in blood stages, it is secreted into the infected erythrocytes and released upon schizont rupture. Mutant *P. berghei* parasites lacking *P*MIF were able to complete the entire life cycle and exhibited no significant changes in growth characteristics or virulence features during blood stage infection. However, rodent hosts infected with knockout parasites had significantly higher numbers of circulating reticulocytes. Our results suggest that *P*MIF is produced by the parasite to influence host immune responses and the course of anemia upon infection.

Cytokines are the molecular messengers of the vertebrate immune system, coordinating the local and systemic immune responses to infective organisms. Macrophage migration inhibitory factor (MIF) was one of the first cytokines to be discovered (4, 17) and is involved in both innate and adaptive immune responses. MIF counterregulates the anti-inflammatory effect of glucocorticoids (9) and is a key regulator of the proinflammatory response to endotoxins. For example, MIF-deficient mice survive a lethal dose of lipopolysaccharide (LPS) (6). MIF is released by immune cells in response to microbial products and proinflammatory cytokines, such as tumor necrosis factor alpha (10, 12). While mammalian MIF is normally found as a homomeric trimer, each subunit has two catalytic sites and two activities: a tautomerase activity, which requires an N-terminal proline residue (33), and an oxidoreductase activity (29), which is based on a thioredoxin-like motif. Although enzymatic activities are not normally found in cytokines, both of these activities have been linked to MIF's cytokine function (28, 38, 45). At the molecular level little is known about the exact mechanisms of MIF function; the biological substrates for the enzymatic activities of MIF, as well as its import and export pathways, are not fully understood. So far, a classical cytokine receptor for MIF has not been discovered, and the surface receptor (CD74) (32) and the intracellular factor Jun activation domain binding protein (Jab-1) (27) are the only functional MIF-binding partners that have been described.

Although the mode of action and the complete biological role of host-derived MIF remain to be established, it has been shown that MIF also has a critical role in determining the outcome of infections caused by parasites such as helminths (42), malaria parasites (34), and *Leishmania* (44). Interestingly, homologues of human MIF (huMIF) have been characterized in nematodes (39, 48, 49). Parasitic nematodes are long lived in their hosts and are able to modulate the immune response to evade killing by the immune system (for a review, see reference 27). Therefore, it has been suggested that the expression of MIF homologues plays a role in the immunobiology of and immune evasion by these nematodes. In support of this, workers have found evidence that nematode MIF has a role in activating macrophages and in recruitment of eosinophils (21). Genome sequencing of other human parasites has revealed that not only parasitic helminths but also protozoans, such as *Plasmodium*, contain genes encoding huMIF homologues (24). *Plasmodium* is the causative agent of malaria, which is responsible for over one million deaths annually and imposes a tremendous social and economic burden (7). The potential ability of *Plasmodium* to manipulate the host immune response though the secretion of cytokine homologues is clearly of interest.

In this paper we describe the first biochemical and genetic characterization of the *Plasmodium* homologues of MIF (*P*MIF) from two species, *Plasmodium falciparum* and *Plasmodium*

* Corresponding author. Mailing address: Department of Parasitology, LUMC, Albinusdreef 2, Room P4-35, 2333 ZA Leiden, The Netherlands. Phone: 31-71 5265069. Fax: 31-71 5266907. E-mail: waters@lumc.nl.

▽ Published ahead of print on 11 December 2006.

berghei. We found that C-terminally His_6-tagged *P*MIF exhibits biochemical and immunostimulatory features similar to those of huMIF and that it is expressed during the blood stages of parasite development in a mammalian host. Furthermore, gene deletion experiments showed that *P. berghei* MIF (*Pb*MIF) is not required for completion of the parasite life cycle but significantly influences the number of reticulocytes in the circulation of mice during the early stages of infection. Furthermore, we found that *P*MIF is secreted from infected red blood cells and ruptured schizonts. Coupled with the lack of an essential intracellular function, therefore, our data indicate that *P*MIF most likely has a function in the interaction of the parasite with its host.

MATERIALS AND METHODS

Plasmid construction. To obtain protein expression constructs, MIF reading frames were amplified from mixed blood stage *P. falciparum* (PlasmoDB entry *Pf*MIF: PFL1420w) and *P. berghei* (GeneDB entry *Pb*MIF: PB000372.03.0) cDNA by PCR using primers L1632 (5′-AAATTTCCGCATGCCGTGCTGTG AATTAATAAC-3′) and L1554 (5′-ATTGGATCCACCAAATAGTGAGCCA CTAAAAGC-3′) (underlining indicates restriction sites) for *P. berghei* and primers L1667 (5′-AAAATTTCCGCATGCCTTGCTGTGAAGTAATAAC-3′) and L1668 5′-ATTGGATCCGCCGAAAAGAGAACCACTGAAGGC-3′ for *P. falciparum*, digested with SphI and BamHI, and ligated into C-terminally His_6-tagged expression vector pQE-70 (QIAGEN). For genomic expression of green fluorescent protein (GFP)-tagged *Pb*MIF, the MIF gene and promoter region (1,200-bp upstream sequence) were amplified from *P. berghei* genomic DNA using primers L1879 (5′-AAAGGTATTCCATGGAACCAAATAGTGAGCCA CTAAAAGCA-3′) and L1880 (5′-TAAATCAAAGCGGCCGCGAATCTTAT CAACCATTTATACC-3′), digested with NcoI and NotI, and ligated into the C-terminally GFP-tagged integration construct pGFP-TAG (30) or pMYC-TAG, which was generated by transferring the c-*myc* tag from pSD141 (41), a kind gift from Oliver Billker (Imperial College, London, United Kingdon), into pGFP-TAG using primers L2300 (5′-CGGGGTACCGCGGCCGCTATCTAG ACGAGGATCCATGGGGCCCGAACAAAAACTCATC-3′) and L2301 (5′-G AGCAGATTGTACTGAGAGTGCACCATATGCGGTG-3′). To obtain a MIF knockout vector, an upstream region (positions −1200 to −300) and a downstream region (positions 785 to 1700) from the *pbmif* gene were amplified from *P. berghei* genomic DNA using primers L1466 (5′-TAAATCAAGGTACC GGCGAATCTTATCAACCATTTATACC-3′) and L1467 (5′-TTGTATTTCA TCGATCTCTTGTGATATTAATCCATACACGCC-3′) and primers L1468 (5′-AAAGAGGCTGAATTCTATGTAAATTATTTTTCCTATGCCCTTAAC-3′) and L1469 (5′-ATCGGATCCTTATGCGTATATATATTGAAGCATGGTG-3′), respectively. The PCR products were digested with Asp718 plus ClaI and EcoRI plus BamHI, respectively, and ligated into B3D (46). All constructs were sequenced to confirm MIF sequence identity.

Protein purification and refolding. *P. falciparum* MIF (*Pf*MIF) and *Pb*MIF were expressed in BL21(DE3)(pLysS) bacteria grown on Luria broth (Q-biogene) containing 30 μg/ml chloramphenicol and 0.05 μg/ml ampicillin. Bacteria were grown at 37°C to an optical density at 600 nm of 0.4 and were induced by addition of isopropyl-D-thiogalactoside to a final concentration of 1 mM. After 3 h, the cells were harvested and lysed in 50 mM Tris (pH 8.0), 500 mM NaCl, 10% (vol/vol) glycerol, 0.01% Nonidet P-40, 10 mM β-mercaptoethanol in the presence of complete protease inhibitor cocktail (Roche) and 1 μg/ml lysozyme. Genomic DNA was fragmented by sonication, after which the lysate was cleared by centrifugation at 30,000 × *g* for 45 min at 4°C and loaded onto an Ni-nitrilotriacetic acid column (QIAGEN) equilibrated in 50 mM Tris (pH 8.0), 200 mM NaCl, 10% (vol/vol) glycerol, 20 mM imidazole, 10 mM β-mercaptoethanol. After washing, the protein was eluted in a linear 20 to 400 mM imidazole gradient. Peak fractions were pooled, concentrated to 10 ml in an Amicon stirred ultrafiltration cell (Millipore) using a 10-kDa-cutoff filter, and loaded on a Superdex 75 gel filtration column (Amersham Pharmacia) equilibrated in 50 mM Tris (pH 8.0), 200 mM NaCl, 5% (vol/vol) glycerol, 5 mM β-mercaptoethanol. These preparations and MIF preparations of refolded lyophilized recombinant MIF (3) were confirmed to be free of LPS (<5 ng of LPS/mg of protein) by the *Limulus* amoebocyte assay (Biowhittaker Inc., Walkersville, MD).

Oxidoreductase and tautomerase assays. Oxidoreductase and tautomerase assays were performed as described previously (29, 43), except that ^1H nuclear magnetic resonance spectra during the tautomerase analysis were recorded with 1-min intervals using a Bruker DPX-300 with 3-(trimethylsilyl)tetradeuteropropionic acid sodium salt as the internal standard.

Antibody generation and Western blotting. Polyclonal antibodies against *Pb*MIF were raised in New Zealand White rabbits by injecting 100 μg LPS-free *Pb*MIF linked to keyhole limpet hemocyanin in complete Freund's adjuvant. After three boosts with 100 μg keyhole limpet hemocyanin-linked *Pb*MIF in incomplete Freund's adjuvant, 5 ml of serum was collected and used at a 1/1,000 dilution as the primary antibody for Western blotting.

Immunofluorescence assays. Blood stages from overnight schizont cultures were fixed with paraformaldehyde, and the c-*myc* tag was visualized by incubation with anti c-*myc* monoclonal antibody (C3956; Sigma-Aldrich, The Netherlands), followed by staining with fluorescein isothiocyanate-labeled goat anti-rabbit immunoglobulin G antibody. Parasite nuclei were stained using 4′,6′-diamidino-2-phenylindole (DAPI) (Sigma-Aldrich, The Netherlands) according to the manufacturer's instructions. Fluorescence was visualized using fluorescence MDR microscopy (GFP and DAPI filter settings; Leica), and images were recorded using a DC500 digital camera.

AP-1 activation assay. The AP-1 assay was performed as described previously (26, 28). Briefly, 1.7×10^5 human embryonic kidney (HEK) cells per well were plated in 24-well cell culture plates. After 24 h, transfection with 50 ng pAP-1-luciferase reporter plasmid and 1 ng pRenilla control plasmid (dual-luciferase reporter assay system; Promega, Leiden, The Netherlands) per 1.7×10^5 HEK cells was performed using lipofectamine 2000 (Invitrogen) as the transfection reagent. Cells were allowed to recover from transfection for 18 h. Then transfected cells were preincubated with recombinant human MIF or *P*MIF or with control buffer for 1 h, followed by an 8-h coincubation with 3 nM phorbol myristate 13-acetate (PMA). Both the PMA concentration and the incubation time were optimized in pilot experiments to obtain the greatest induction of the AP-1 promoter without causing significant cell death. Control cells (basal) were not incubated with PMA. Cells were washed, and cell lysates were prepared using 100 μl passive lysis buffer (dual-luciferase reporter assay system; Promega) to quantify luciferase and renilla activities according to the protocol of the manufacturer.

Gene knockout and tagging in *P. berghei*. Transfection and selection of parasites with *pbmif* deleted or of tagged parasites were performed as previously described (18). Genomic integration of knockout and tagging vector DNA was confirmed by Southern blotting of pulse-field gel electrophoresis-separated chromosomes of the knockout or tagged parasites and probing with the 3′ untranslated region of the PbDHFR gene. In addition, correct replacement of the *Pb*MIF locus was verified by Southern blotting of AccI- and AccI/XbaI-digested wild-type and *pbmif* knockout (*pbmif*-ko) parasite genomic DNA and probing with the upstream *pbmif* knockout target region (positions −1200 to −300). The *pbmif*-ko lines and the line expressing c-*myc*-tagged *Pb*MIF were cloned using limiting dilution, whereas the line expressing GFP-tagged *Pb*MIF was not cloned using limiting dilution.

Virulence experiments. In two experiments, five hosts (mouse strains BALB/c and C57BL/6) were infected with HP-ANKA wild-type *P. berghei* parasites and five hosts were infected with *pbmif*-ko parasites (*pbmif*-ko1). In addition, in the second experiment, five hosts for both mouse strains were also infected with a second independently generated *pbmif*-ko parasite line (*pbmif*-ko2). All parasite lines were generated from the same stock (passage number). All mice (Haarlan, United Kingdom) were randomized into groups with respect to weight and red blood cell count, infected intraperitoneally with 1×10^5 ring stage parasites, and monitored daily from day 3 postinfection. Every day of sampling, mice were weighed, thin smears were prepared, and the red blood cell densities were calculated by flow cytometry (the mature red blood cells and reticulocytes in the size range from 3.3 to 10 μm in diameter in 2 μl of tail blood were counted according to the manufacturer's instructions; Coulter Electronics, United Kingdom). Mice were sampled until the level of parasitemia became very high (>50%) and/or substantial mortality occurred (day 12 postinfection for BALB/c hosts and day 7 postinfection for C57BL/6 hosts).

Analysis of virulence experiments. The proportion of parasitized red cells (parasitemia) and the proportion of red cells that were reticulocytes (reticulocytemia) were calculated daily from thin smears, and the results were transformed to obtain parasite and reticulocyte densities using red cell density counts. The following summary statistics for each infected host were calculated: cumulative densities for parasites and reticulocytes; red cell and mass loss; minimum red cell density and mass; and peak parasitemia and reticulocytemia. Proportion data were arcsin square root transformed to comply with the assumptions of parametric tests. For all experiments, general linear models (R Foundation for Statistical Computing, Austria) were used to compare infection parameters for *pbmif*-ko and wild-type infections, and Tukey tests were used to determine which groups differed when significant results were obtained.

FIG. 1. Sequence alignment of mammalian and parasite MIFs. (A) Sequence alignment of human, mouse, *P. berghei* (Pb), and *P. falciparum* (Pf) MIF homologues, as well as two *Brugia malayi* MIF homologues (Bm-1 and -2). The arrow indicates the N-terminal catalytic proline associated with tautomerase activity, and the area enclosed in a box is the CXXC motif associated with oxidoreductase activity in the mammalian MIFs and the parasite variants. Asterisks indicate identical residues; colons and dots indicate residues with high and low levels of similarity, respectively. (B) Ribbon representation of the huMIF crystal structure (RCSB PDB entry: 1CA7 [33]). For clarity, only one monomer of the trimer is shown. Arrows indicate the positions of the tautomerase and oxidoreductase active sites. The first cysteine of the CXXC oxidoreductase motif (C57 in huMIF) that is conserved in the parasite MIFs is red. Conserved residues in the various MIFs mainly cluster around the tautomerase active site and are shown in ball-and-stick form.

RESULTS

MIF is expressed constitutively by *Plasmodium* and secreted by blood stage forms. MIF homologues have been found previously in a number of parasitic nematodes (21, 48, 49) and have now also been found in apicomplexans, including *Plasmodium* (PlasmoDB entry *Pf*MIF: PFL1420w; GeneDB entry *Pb*MIF: PB000372.03.0). These parasite MIFs exhibit moderate levels of homology with mammalian MIFs and with each other (29% identity and 39% similarity between huMIF and *Pf*MIF) (Fig. 1A). Nevertheless, a crystal structure determination of nematode MIF protein revealed that the overall structure of the divergent MIF proteins is highly conserved (45), and thus the sequence of parasite MIFs can be accurately threaded onto the human MIF structure. Conserved residues, shown in Fig. 1B in ball-and-stick form in the crystal structure of huMIF (33), mainly cluster around the tautomerase active site (residues 2, 32 to 34, and 64 to 66), indicating that the tautomerase activity is likely to be a shared property of mammalian and parasite MIFs. In contrast, the second cysteine in the mammalian MIF CXXC oxidoreductase motif does not seem to be as well conserved in the parasite MIFs (Fig. 1A).

To determine the expression profile of *Pb*MIF, we analyzed *P. berghei* infection at various stages by Northern blotting. *pbmif* was transcribed throughout the asexual blood stages, and peak steady-state mRNA levels were observed at the late trophozoite and early schizont stages (Fig. 2A). Furthermore, we

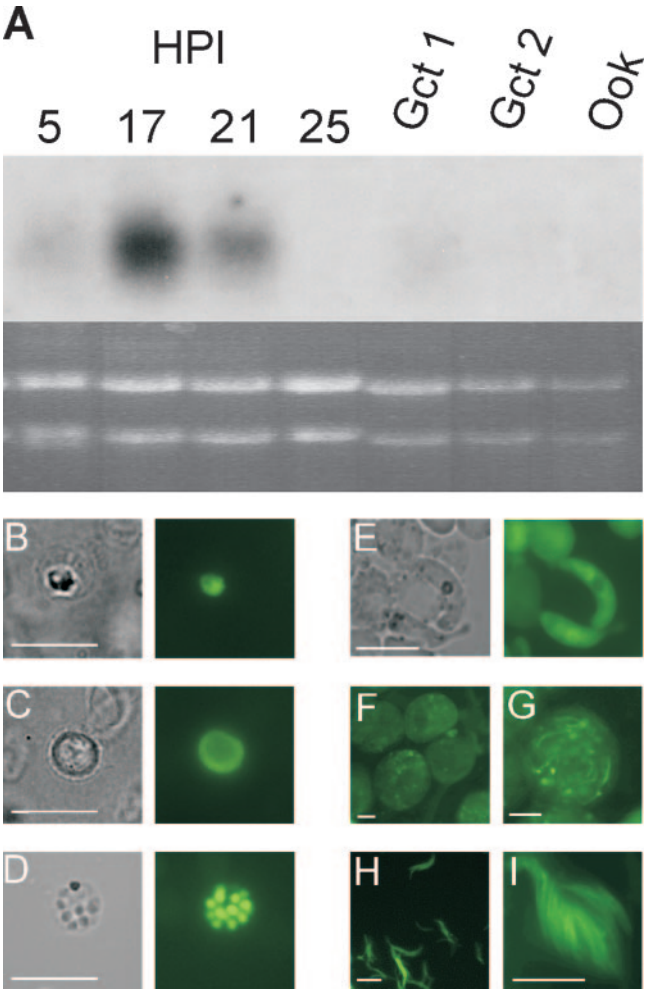

FIG. 2. Expression of *Pb*MIF throughout the life cycle. (A) Time course Northern analysis of the *Pb*MIF transcript in blood stages. Whole RNA extracted at various times from a synchronous *P. berghei* blood stage infection showed that there was production of *Pb*MIF mRNA of the expected size (~0.7 kb) at 17 h postinfection (HPI) (trophozoite stage). Small quantities of transcript were also present in the sexual stages (Gct 1, enriched gametocytes; Gct 2, purified gametocytes) and the ookinete (Ook). An ethidium bromide-stained portion of the gel showing the positons of the 28S and 18S rRNAs was included as loading control. (B to E) Protein expression of the *Pb*MIF-GFP fusion throughout the life cycle in a late ring/early trophozoite (B), mature trophozoite (C), schizont (D), and mature ookinete (some unfertilized female gametes are also visible) (E). Magnification, ×100. (F and G) Protein expression of the *Pb*MIF-GFP fusion in a day 18 oocyst. Magnification, ×20 and ×40, respectively. (H and I) Protein expression of the *Pb*MIF-GFP fusion in salivary gland sporozoites. Magnification, ×40 and ×100, respectively. Bars, 10 μm.

tracked *Pb*MIF protein expression by examining generation of a knockin *P. berghei* strain expressing C-terminally GFP-tagged *Pb*MIF under control of the endogenous promoter (Fig. 3B). Since the molecular weight of the GFP tag is about three times the molecular weight of the *Pb*MIF monomer, the presence of GFP may affect the cellular distribution of *Pb*MIF. Therefore, we did not draw any conclusion with regard to cellular localization of the fusion, other than presence or absence at a given stage of the life cycle. *Pb*MIF-GFP was found to be expressed ubiquitously in the blood stages and in mosquito stage ookinetes and sporozoites (Fig. 2B to I).

Any function of *P*MIF in a parasite-host interaction or in immune evasion would require *P*MIF to be externalized by the parasite. However, like mammalian MIF, which is exported by nonclassical pathways likely involving an ABCA1 transporter (22), *P*MIF has no signal sequence. To analyze whether *P*MIF is released from parasite-infected erythrocytes, we developed a polyclonal antibody specific for *Pb*MIF and immunoblotted supernatants and lysates of synchronous, cultured *P. berghei* blood stage parasites. This antibody showed extremely low cross-reactivity with recombinant huMIF during a long exposure (>5 min) of the blot (Fig. 4A, lanes 12 and 13), which is virtually identical to the results obtained with murine MIF (89% identity and 95% homology). Nevertheless, to prevent any confounding presence of murine MIF, we removed all leukocytes by passing the sample over a Plasmodipur filter (Euro-Diagnostica, Arnhem, The Netherlands). When grown in culture, *P. berghei* blood stage parasites arrest in the late schizont stage, since the infected erythrocytes do not rupture (47). This allows workers to discriminate between active secretion throughout asexual growth and release by the infected erythrocyte at the time of schizont rupture. Figure 4A shows that significant levels of *Pb*MIF were present in the cytoplasm of the infected erythrocytes in both the trophozoite and schizont stages. A small quantity of *Pb*MIF was also detected in the culture supernatant, but the amount varied between experiments (not shown), so the MIF was likely released by mechanical shearing of infected erythrocytes. Mechanical rupture of the parasitophorous vacuole of the schizonts, releasing the merozoites, resulted in release of an additional burst of *Pb*MIF. Lysis of trophozoites or merozoites released additional MIF.

Rabbit polyclonal *Pb*MIF antisera showed high nonspecific cross-reactivity in an immunofluorescence assay, precluding direct visualization of *Pb*MIF in infected cells. Therefore, a knockin *P. berghei* strain expressing *Pb*MIF with the much smaller (2.7-kDa) C-terminal c-*myc* tag (Fig. 3B) was generated, enabling direct detection of the fusion using monoclonal anti-c-*myc* antibodies. Figure 4B1 shows staining of the parasitophorous vacuole in trophozoites and schizonts, along with faint staining of the infected erythrocyte cytoplasm in the trophozoite. Schizont rupture resulted in a loss of fluorescence (Fig. 4B2), consistent with the results shown in Fig. 4A.

Expression and purification of recombinant *P*MIF-His$_6$ and measurement of enzymatic activities. Although all MIFs are structurally conserved, the conservation of the residues associated with the two known enzymatic activities is greater for the tautomerase activity than for the oxidoreductase activity. Since the N-terminal proline is the catalytic residue in the tautomerase activity (33) and we wanted to compare the enzymatic properties of *P*MIF with those of huMIF, we located the His$_6$ tag at the C terminus well away from any enzymatic site in our *Pb*MIF, *Pf*MIF, and huMIF expression constructs. The major peak of *P*MIF-His$_6$ eluted at an apparent molecular mass of 30 kDa on a size exclusion column, while huMIF-His$_6$ eluted at an apparent molecular mass of 22 kDa. Both values are consistent with a dimeric form in solution (Fig. 5A). We determined the tautomerase activity of the purified recombinant *P*MIF-His$_6$ by monitoring the conversion of *p*-hydroxy-

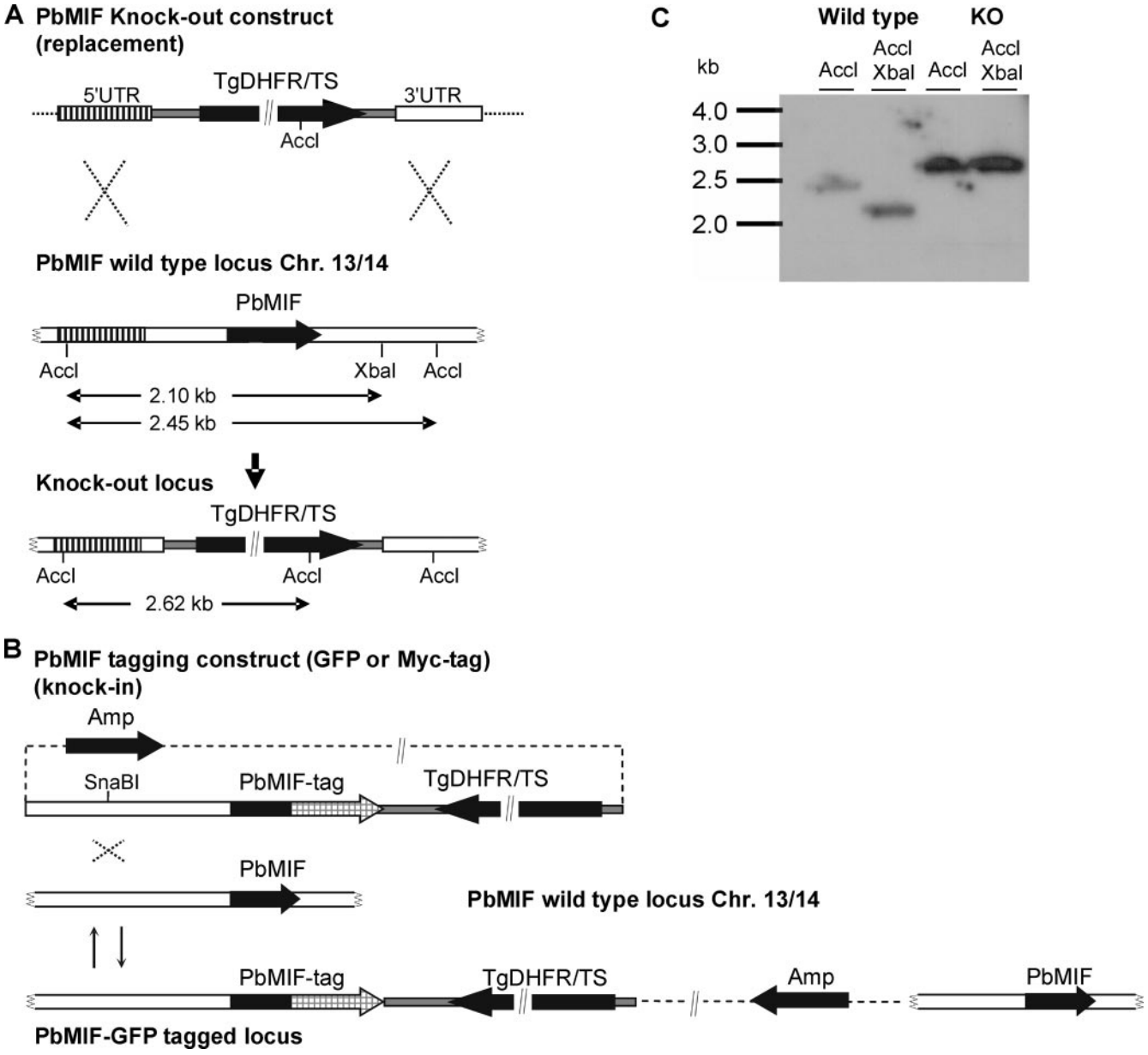

FIG. 3. Genetic manipulation of the *pbmif* locus. (A) *pbmif*-ko was made by double-crossover replacement using the 5′ untranslated region (5′UTR) (positions −1200 to −300) and 3′ untranslated region (3′UTR) (positions 785 to 1700) from the *pbmif* gene. Gene replacement with the TgDHFR/TS selection marker removed the XbaI site in the 3′ untranslated region of *Pb*MIF and introduced an additional AccI site. The sizes of restriction fragments are indicated between arrows, and the hatched box represents the region that was used as a probe in the Southern analysis whose results are shown in panel C. (B) *Pb*MIF-GFP and c-*myc* fusions were made by a single-crossover knockin (insertion) event, which resulted in gene duplication of *pbmif* with one of the two copies tagged with GFP or c-*myc*, while the second copy remained wild type. (C) Southern blot analysis of AccI- and AccI/XbaI-digested genomic DNA from wild-type and knockout parasites. Using the 5′ untranslated region integration target (hatched box in panel A) as the probe, the digestions should have yielded 2,447-, 2,100-, 2,616-, and 2,616-bp fragments, respectively.

phenylpyruvate from the enol form to the keto form by ^{1}H nuclear magnetic resonance (43). *Pf*MIF-His$_6$ and *Pb*MIF-His$_6$ showed levels of tautomerase activity that were appreciably above the background level of the mock purification control, but the activity was fivefold lower that the activity of wild-type huMIF-His$_6$, which was used as a control (Fig. 5B). We next tested whether *P*MIF-His$_6$ exhibited oxidoreductase activity and quantified the NADPH-dependent reduction of 2-hydroxyethyldisulfide (HED). Figure 5C shows that the oxidoreductase activity of *Pf*MIF-His$_6$ was able to catalyze the reduction of HED at levels greater than the levels observed for the mock purification control. Surprisingly, given the lack of conservation, the oxidoreductase activity was also reduced only about fivefold compared to the activity of the huMIF-His$_6$ wild-type control. In both assays, *Pb*MIF-His$_6$ exhibited less activity than *Pf*MIF-His$_6$ exhibited. Given the high level of conservation between these two MIFs, however, this was unlikely to be due to lower intrinsic activity

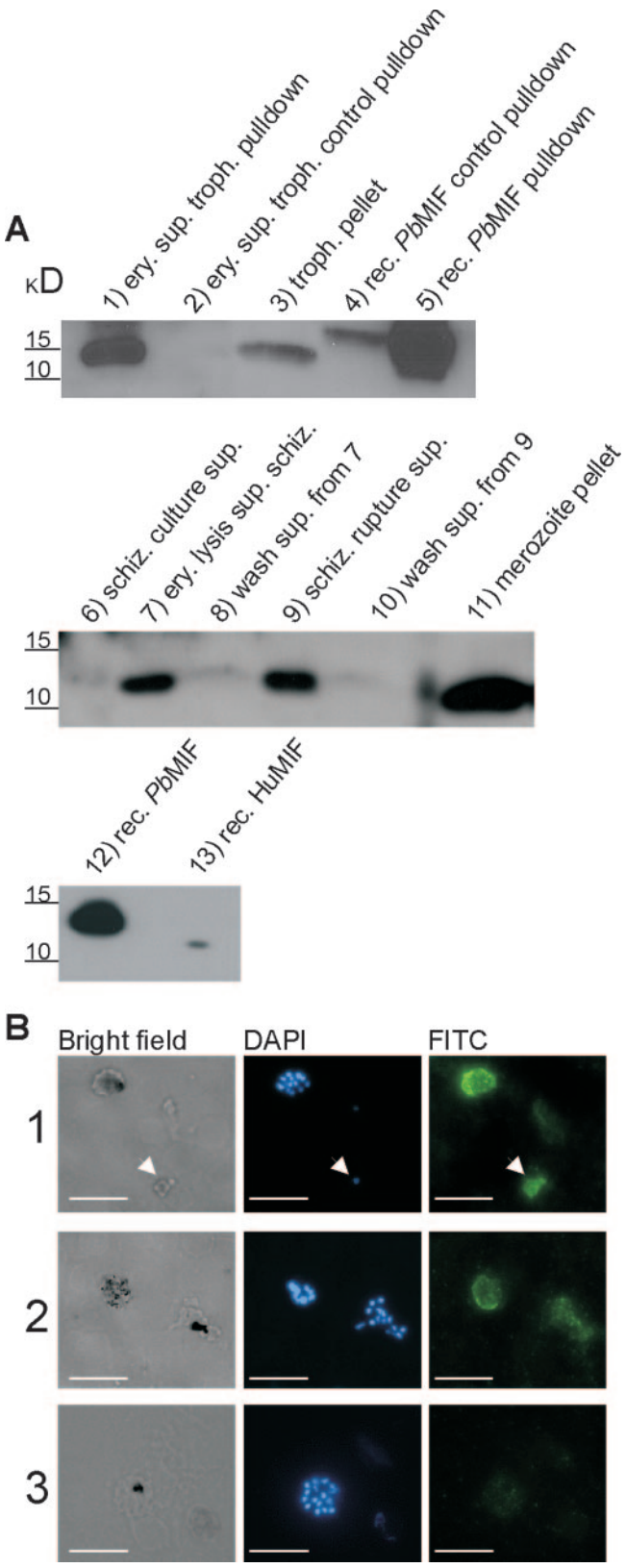

FIG. 4. *Pb*MIF is externalized by *P. berghei* and is released upon schizont rupture. (A) Western blot analysis using anti-*Pb*MIF rabbit polyclonal antiserum. Lane 1 contained erythrocytes (ery.) infected with trophozoite (troph.) stage *P. berghei* that were isolated by heart puncture and lysed by osmotic shock. Parasite-derived MIF was pulled down from the lysis supernatant (sup.) (from the equivalent of 10^7 infected erythrocytes) using anti-*Pb*MIF bound to protein G-Sepharose. Lane 2 contained control pulldown of the lysis supernatant using protein G-Sepharose alone. Lane 3 contained a trophozoite pellet ($\sim 2.0 \times 10^5$ parasites loaded). Lane 4 contained control pulldown of 100 ng of recombinant (rec.) C-terminally His_6-tagged *Pb*MIF using protein G-Sepharose alone. Lane 5 contained control pulldown of 100 ng of recombinant C-terminally His_6-tagged *Pb*MIF using anti-*Pb*MIF loaded protein G-Sepharose. Lane 6 contained supernatant (10 μl of 100 ml) of an overnight schizont (schiz.) culture. Lane 7 contained supernatant (10 μl of 20 ml) of schizonts after disruption of the host erythrocyte membrane. Lane 8 contained phosphate-buffered saline wash supernatant (10 μl of 1 ml) of schizont pellet from lane 7. Lane 9 contained supernatant (10 μl of 1 ml) after mechanical rupturing of the schizonts into merozoites. Lane 10 contained phosphate-buffered saline wash supernatant (10 μl of 1 ml) of the merozoites from lane 9. Lane 11 contained solubilized merozoite pellet ($\sim 2.0 \times 10^5$ parasites loaded). Lane 12 contained 50 ng of recombinant C-terminally His_6-tagged *Pb*MIF. Lane 13 contained 100 ng of recombinant huMIF. (B) Immunofluorescent detection of c-*myc*-tagged *Pb*MIF in blood stages. Thin smears from an overnight schizont culture expressing *Pb*MIF–c-*myc* were stained using an anti-c-*myc* monoclonal antibody. (Panel 1) Intact schizont and trophozoite (arrowhead) show staining within the parasitophorous vacuole. (Panel 2) Intact schizont and ruptured schizont. (Panel 3) Wild-type *P. berghei* control stained with the anti-c-*myc* monoclonal antibody. The fluorescent image in panel 3 was taken with a 0.6-s exposure, while the fluorescent images in panels 1 and 2 were taken with a 0.3-s exposure. Bars, 10 μm. FITC, fluorescein isothiocyanate.

but rather may have reflected small differences in refolding efficiency.

Recombinant *P*MIF is as efficient as huMIF in inhibiting AP-1 stimulation. We investigated if the in vivo activity of *P*MIF-His_6 mirrored the reduced enzymatic activity of *P*MIF-His_6 compared to huMIF-His_6 activity. huMIF can reduce AP-1 expression by physically interacting with the transcriptional coactivator Jab-1, an activity at least partially dependent on the oxidoreductase activity of huMIF (28). Therefore, we used an AP-1 reporter assay with HEK cells to examine the biological activity of recombinant *P*MIF-His_6. Figure 6 shows that although both huMIF-His_6 and *P*MIF-His_6 showed a trend toward repression of the basal expression of AP-1, this effect became statistically relevant ($P < 0.05$; $n \geq 6$) only after AP-1 expression was induced with PMA. The induction of the AP-1 promoter by PMA was quite subtle in HEK cells. Higher levels of induction could be obtained by increasing the PMA concentration and incubation time, but they were invariably associated with increased cell death. Nevertheless, the repression effect was on the same order of magnitude for both huMIF-His_6 and *P*MIF-His_6, which implies that *P*MIF is able to bind to and interfere with Jab-1 to the same extent as huMIF despite its reduced oxidoreductase activity.

***Pb*MIF knockout parasites are viable throughout the life cycle and increase host reticulocyte density.** To investigate the role of *Pb*MIF during in vivo infection in the mouse host and mosquito vector, two independent *pbmif*-ko parasite lines were generated using double-crossover gene replacement. Correct integration of the selection marker and disruption of the *pbmif* locus were confirmed by pulse-field gel electrophoresis, PCR (not shown), and Southern blotting (Fig. 3). *pbmif*-ko parasites were viable in vivo, replicated asexually at the same rate as

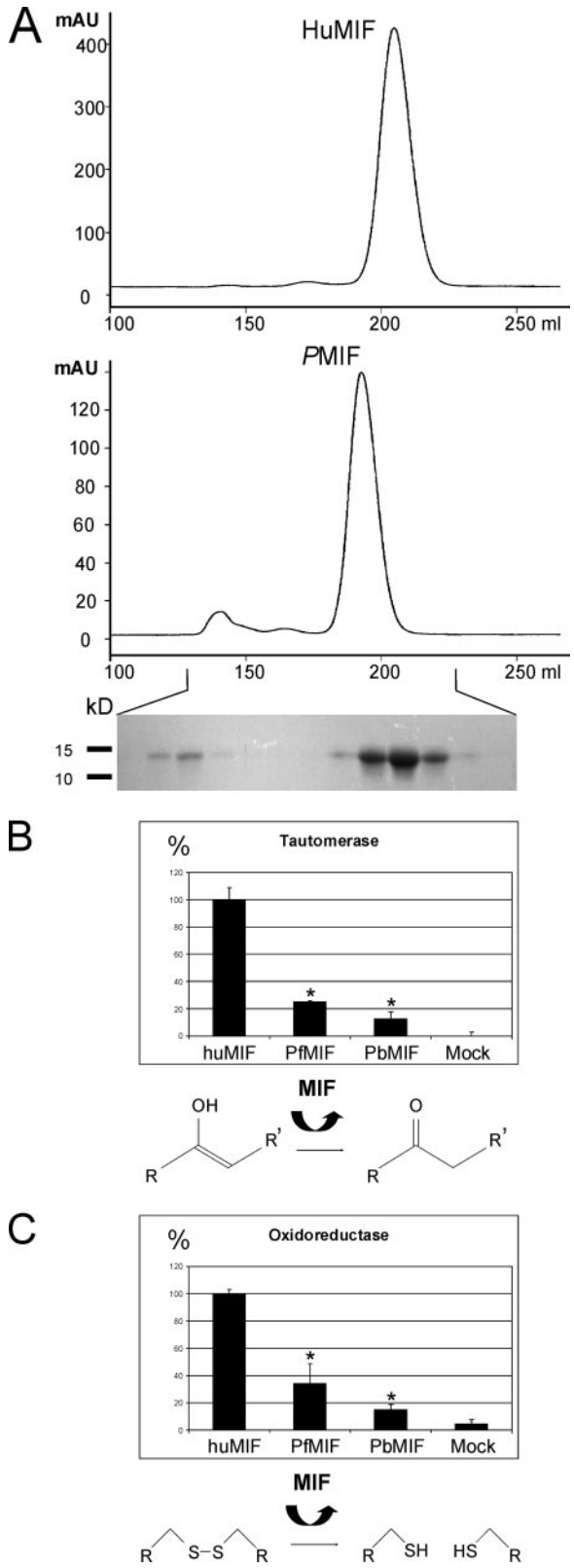

FIG. 5. Recombinant *P*MIF elutes as a dimer in size exclusion chromatography and is active in tautomerase and oxidoreductase assays. (A) Chromatograms of C-terminally His_6-tagged huMIF and *Pb*MIF. The retention volume of the major peak for C-terminally His_6-tagged *Pb*MIF was 192.10 ml, compared to 204.87 ml for C-terminally His_6-tagged huMIF, which resulted in calculated molecular masses of 30 kDa for *Pb*MIF and 22 kDa for huMIF. The reference compounds included bovine albumin (66 kDa; 153.93 ml), chicken ovalbumin (45 kDa; 170.93 ml), bovine carbonic anhydrase (30 kDa; 192.47 ml), and bovine α-lactalbumin (14.4 kDa; 217.39 ml). The inset shows a Coomassie blue-stained protein gel containing the peak fractions for *Pb*MIF, which identified the void volume peak as *Pb*MIF aggregates. The same results were obtained with *Pf*MIF (data not shown). mAU, milli-absorbance units. (B and C) Recombinant MIF tautomerase activity with *p*-hydroxyphenylpyruvate (R = COOH and R′ = C_6H_4-OH) (B) and oxidoreductase activity with 2-hydroxyethyldisulfide (R = CH_2-OH) (C). Sample equations are shown for both conversions. The activities of *Pf*MIF and *Pb*MIF are expressed as percentages of the huMIF activity. In both sets of experiments, the *Pf*MIF and *Pb*MIF activities were greater than the activities of the mock purification control. Asterisks indicate that the *P* value is <0.05 ($n \geq 3$).

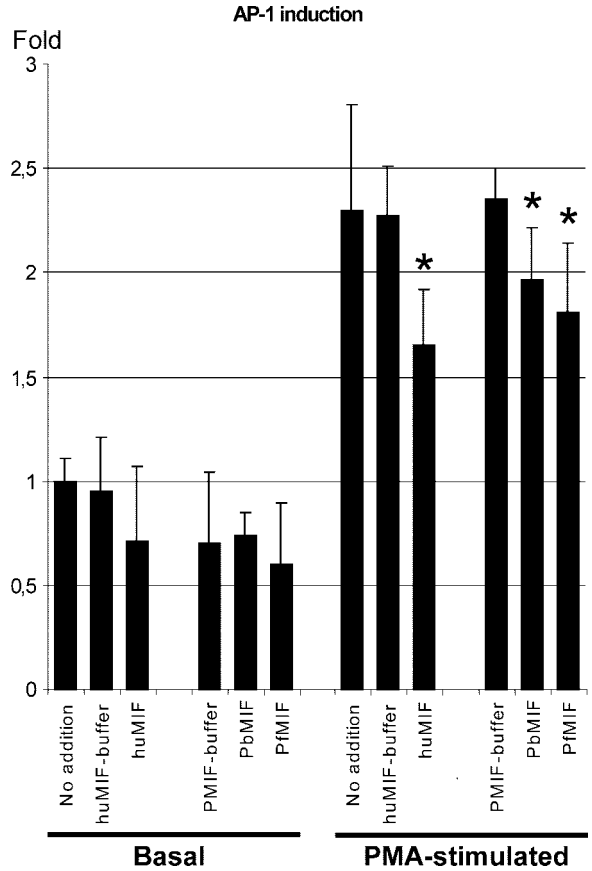

FIG. 6. Recombinant *P*MIF can inhibit AP-1 induction like huMIF. At the basal level of transcription, both huMIF and *P*MIF showed a nonsignificant trend toward inhibition of AP-1 transcription in HEK cells. However, upon stimulation with PMA, both huMIF and *P*MIF showed statistically relevant repression compared to buffer controls. Asterisks indicate that the *P* value is <0.05 ($n \geq 6$).

wild-type parasites, formed sexual stage parasites at the wild-type frequency, and were transmitted throughout the full life cycle (not shown). Since *Pb*MIF may have a more subtle role in parasite-host interactions, we investigated *pbmif*-ko parasite

TABLE 1. Comparison of virulence parameters for infections with wild-type and *pbmif*-ko parasites[a]

Host mice	Variable	Test statistics	Further details
BALB/c	Cumulative parasite density	$F_{(1,8)} = 0.59$; $P = 0.464$	Wild type infections: 1.04 ± 0.15 *pbmif*-ko1 infections: 0.68 ± 0.16
	Peak parasitemia	$F_{(1,8)} = 5.00$; $P = 0.056$	Wild type infections: 7.24 ± 1.03 *pbmif*-ko1 infections: 4.88 ± 1.20
	Minimum mass	$F_{(1,8)} = 3.04$; $P = 0.119$	Wild type infections: 17.74 ± 0.53 *pbmif*-ko1 infections: 18.38 ± 0.19
	Minimum red blood cell density	$F_{(1,8)} = 0.20$; $P = 0.668$	Wild type infections: 8.00 ± 0.29 *pbmif*-ko1 infections: 8.29 ± 0.22
	Cumulative reticulocyte density	**$F_{(1,8)} = 44.0$; $P < 0.001$**	Wild-type-infected hosts had significantly fewer reticulocytes (0.18 ± 0.02) than *pbmif*-ko1-infected hosts (0.79 ± 0.10)
	Peak reticulocytemia	**$F_{(1,8)} = 48.6$; $P < 0.001$**	Wild-type-infected hosts had significantly lower peak reticulocytemia (1.02 ± 0.07) than *pbmif*-ko1-infected hosts (3.32 ± 0.45)
C57BL/6	Cumulative parasite density	$F_{(1,7)} = 2.63$; $P = 0.149$	Wild type infections: 2.14 ± 0.22 *pbmif*-ko1 infections: 1.72 ± 0.15
	Peak parasitemia	$F_{(1,7)} = 3.86$; $P = 0.091$	Wild type infections: 14.83 ± 1.78 *pbmif*-ko1 infections: 11.18 ± 1.02
	Minimum mass	$F_{(1,7)} = 2.75$; $P = 0.142$	Wild type infections: 17.07 ± 0.44 *pbmif*-ko1 infections: 18.56 ± 0.71
	Minimum red blood cell density	$F_{(1,7)} = 1.26$; $P = 0.299$	Wild type infections: 6.93 ± 0.46 *pbmif*-ko1 infections: 7.58 ± 0.37
	Cumulative reticulocyte density	**$F_{(1,7)} = 8.74$; $P = 0.021$**	Wild-type-infected hosts had significantly fewer reticulocytes (1.31 ± 0.14) than *pbmif*-ko1-infected hosts (1.90 ± 0.15)
	Peak reticulocytemia	**$F_{(1,7)} = 5.57$; $P = 0.0503$**	There was a borderline trend for the peak reticulocytemia of wild-type-infected hosts (10.4 ± 0.84) to be marginally higher than the peak reticulocytemia of *pbmif*-ko1-infected hosts (8.12 ± 0.63). However, the mean reticulocytemia was higher in *pbmif*-ko1-infected hosts on 3 of the 4 days examined. Therefore, this trend does not contradict the reticulocyte density results.

[a] Results of experiment 1, in which BALB/c hosts and C57BL/6 hosts were infected with either wild-type or *pbmif*-ko1 parasites. The statistics are from general linear models, and the F ratio represents the variance attributable to each explanatory variable when the variance remaining unexplained by the model was compared. This ratio was weighted by the degrees of freedom associated with each explanatory variable and compared to the appropriate F distribution to generate the *P* value. For all variables, means and standard errors are shown. Variables for which wild-type infections differed significantly from *pbmif*-ko infections are indicated by boldface, and further explanation is provided. The units are percentages for proportion data and 10^9 cells/ml for density data.

virulence and infection dynamics in two inbred mouse strains, BALB/c and C57BL/6.

In C57BL/6 mice, *P. berghei* ANKA infection (intraperitoneal injection of 1×10^5 parasites) generally leads to cerebral complications, presenting as ataxia, shivering, lethargy, and death at days 8 to 9 after infection as the level of parasitemia reaches ~10% (16, 20). *P. berghei* ANKA infection in BALB/c mice may lead to similar cerebral complications in a small proportion of mice or, more commonly, to a syndrome termed severe malaria (19, 20), in which mice suffer from severe anemia, weight loss, and organ damage from day 8 after infection that are associated with a high level of parasitemia. Mice infected with wild-type or *pbmif*-ko parasites had symptoms consistent with these syndromes; infection of C57BL/6 mice resulted in death at day 8 postinfection, and infection of BALB/c mice resulted in high levels of parasitemia and severe anemia (Tables 1 and 2) in all cases.

In both experiments, with two independently generated *pbmif*-ko lines and two mouse strains, hosts infected with the *pbmif*-ko lines had significantly higher reticulocyte densities and peak levels of reticulocytemia than hosts infected with wild-type parasites (Fig. 7; Tables 1 and 2). In contrast, none of the other virulence parameters revealed consistently significant differences between infections with *pbmif*-ko parasites and infections with wild-type parasites. In both experiments, infections with the first *pbmif*-ko line (*pbmif*-ko1) did not differ significantly from infections with wild-type parasites in terms of cumulative parasite density, peak parasitemia, minimum mass, mass loss, minimum red cell density, or red cell loss. When infections initiated with the second *pbmif*-ko line (*pbmif*-ko2) were compared to infections with wild-type parasites, there were no significant differences in peak parasitemia, minimum mass, mass loss, or red cell loss. However, compared to infections with wild-type parasites, for infections with *pbmif*-ko2 parasites the cumulative parasite densities were significantly higher, but only in BALB/c mice, and the minimum red cell

TABLE 2. Comparison of virulence parameters for infections with wild-type and two independently generated *pbmif*-ko parasites[a]

Host mice	Variable	Test statistics	Further details
BALB/c	**Cumulative parasite density**	**$F_{(2,12)} = 8.32$; $P = 0.005$**	Wild-type parasites (0.13 ± 0.04) did not reach significantly different densities than *pbmif*-ko1 parasites (0.28 ± 0.09), but *pbmif*-ko2 parasites (0.76 ± 0.16) reached significantly higher densities than both other genotypes. The data do not show a consistent trend for *pbmif*-ko parasites to reach higher densities than wild-type parasites.
	Peak parasitemia	$F_{(2,12)} = 0.06$; $P = 0.946$	Wild type infections: 12.90 ± 2.32 *pbmif*-ko1 infections: 9.61 ± 2.14 *pbmif*-ko2 infections: 11.74 ± 2.59
	Minimum mass	$F_{(2,12)} = 0.44$; $P = 0.653$	Wild type infections: 17.57 ± 0.38 *pbmif*-ko1 infections: 17.05 ± 0.44 *pbmif*-ko2 infections: 16.73 ± 0.87
	Mass loss	$F_{(2,12)} = 0.11$; $P = 0.901$	Wild type infections: 3.33 ± 0.52 *pbmif*-ko1 infections: 3.08 ± 0.84 *pbmif*-ko2 infections: 2.87 ± 0.67
	Minimum red blood cell density	$F_{(2,12)} = 0.18$; $P = 0.835$	Wild type infections: 5.07 ± 0.43 *pbmif*-ko1 infections: 5.04 ± 0.23 *pbmif*-ko2 infections: 4.79 ± 0.39
	Red blood cell loss	$F_{(2,12)} = 0.14$; $P = 0.871$	Wild type infections: 5.21 ± 0.84 *pbmif*-ko1 infections: 4.91 ± 0.29 *pbmif*-ko2 infections: 5.36 ± 0.54
	Cumulative reticulocyte density	**$F_{(2,12)} = 17.69$; $P < 0.001$**	Wild-type-infected hosts had significantly fewer reticulocytes (1.13 ± 0.07) than *pbmif*-ko1-infected hosts (2.51 ± 0.25) and *pbmif*-ko2-infected hosts (2.28 ± 0.15)
	Peak reticulocytemia	**$F_{(2,12)} = 24.00$; $P < 0.001$**	Wild-type-infected hosts had significantly lower peak levels of reticulocytes (2.10 ± 0.22) than *pbmif*-ko1-infected hosts (4.24 ± 0.35) and *pbmif*-ko2-infected hosts (5.56 ± 0.57)
C57BL/6	Cumulative parasite density	$F_{(2,12)} = 0.95$; $P = 0.415$	Wild type infections: 0.67 ± 0.15 *pbmif*-ko1 infections: 0.50 ± 0.10 *pbmif*-ko2 infections:0.79 ± 0.19
	Peak parasitemia	$F_{(2,12)} = 1.93$; $P = 0.188$	Wild type infections: 6.48 ± 1.54 *pbmif*-ko1 infections: 5.18 ± 1.27 *pbmif*-ko2 infections: 10.36 ± 2.70
	Minimum mass	$F_{(2,12)} = 1.97$; $P = 0.182$	Wild type infections: 16.42 ± 0.42 *pbmif*-ko1 infections: 16.53 ± 0.46 *pbmif*-ko2 infections: 16.41 ± 0.30
	Mass loss	$F_{(2,12)} = 0.03$; $P = 0.975$	Wild type infections: 0.34 ± 0.17 *pbmif*-ko1 infections: 0.82 ± 0.15 *pbmif*-ko2 infections: 0.94 ± 0.32
	Minimum red blood cell density	**$F_{(2,12)} = 11.84$; $P = 0.001$**	*pbmif*-ko2-infected hosts were more anemic (4.74 ± 0.29) than wild-type-infected hosts (7.27 ± 0.35). *pbmif*-ko1-infected hosts (5.86 ± 0.43) did not have significantly different minimum red cell densities than wild-type-infected hosts. Therefore, there was not a consistent trend for *pbmif*-ko-infected hosts to be less anemic than wild-type-infected hosts.
	Red blood cell loss	$F_{(2,12)} = 2.28$; $P = 0.102$	Wild type infections: 2.33 ± 0.20 *pbmif*-ko1 infections: 2.75 ± 0.84 *pbmif*-ko2 infections: 4.15 ± 0.48
	Cumulative reticulocyte density	**$F_{(2,12)} = 8.61$; $P = 0.005$**	Wild-type-infected hosts had significantly fewer reticulocytes (0.41 ± 0.10) than *pbmif*-ko1-infected hosts (1.57 ± 0.30) and *pbmif*-ko2-infected hosts (1.36 ± 0.18)
	Peak reticulocytemia	**$F_{(2,12)} = 7.93$; $P = 0.006$**	Wild-type-infected hosts had significantly lower peak levels of reticulocytes (2.20 ± 0.58) than *pbmif*-ko1-infected hosts (10.07 ± 2.35) and *pbmif*-ko2-infected hosts (9.23 ± 1.77)

[a] Results of experiment 2, in which in which BALB/c hosts and C57BL/6 hosts were infected with either wild-type parasites or one of two independent lines of *pbmif*-ko parasites (*pbmif*-ko1 and *pbmif*-ko2). The statistics are from general linear models, and the F ratio represents the variance attributable to each explanatory variable when the variance remaining unexplained by the model was compared. This ratio was weighted by the degrees of freedom associated with each explanatory variable and compared to the appropriate F distribution to generate the *P* value. For all variables, means and standard errors are shown. Variables for which wild-type infections differed significantly from *pbmif*-ko infections are indicated by boldface, and further explanation is provided. The units are percentages for proportion data and 10^9 cells/ml for density data.

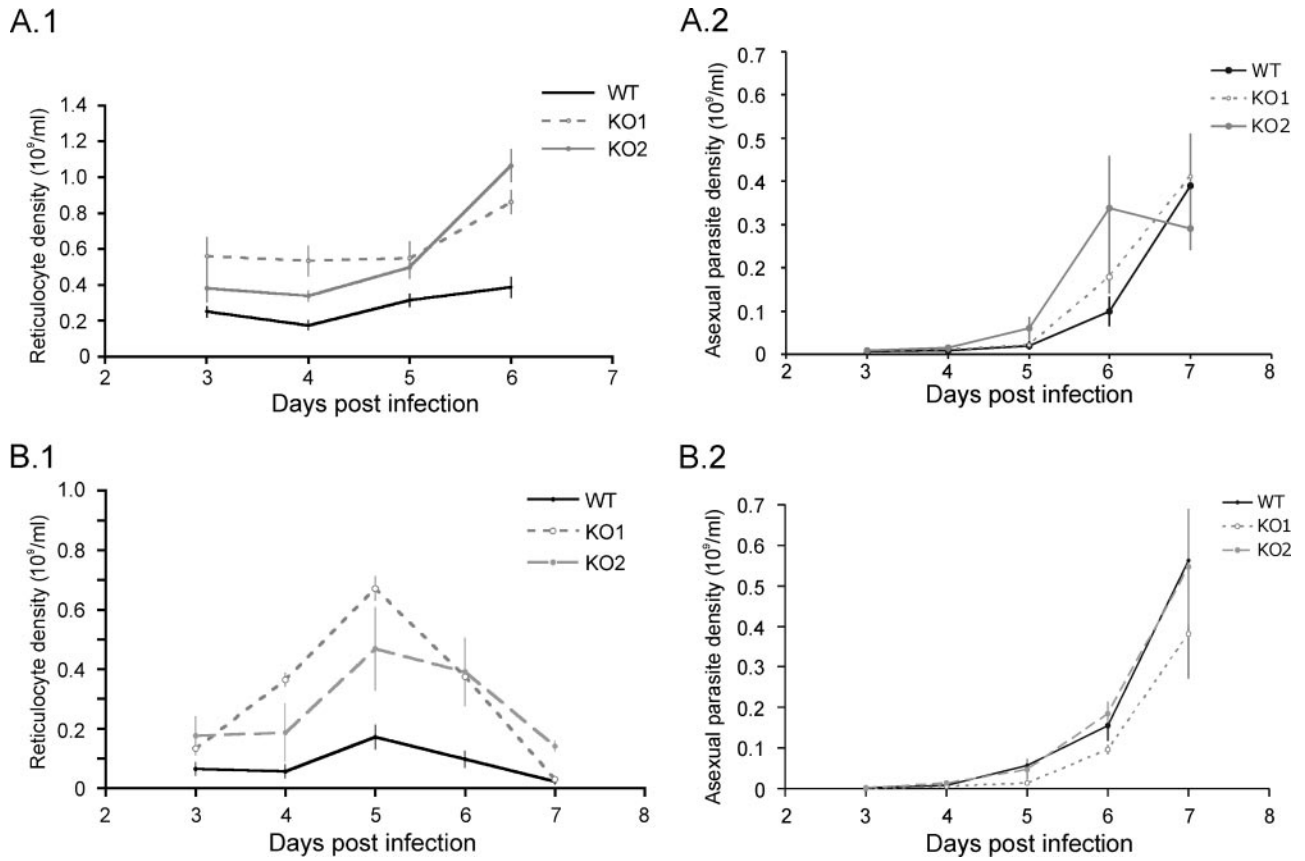

FIG. 7. Parasite and reticulocyte densities in *pbmif*-ko-infected mice. The values are means and standard errors for asexual stage and reticulocyte density during infections in experiment 2, obtained by using BALB/c mice (A.1 and A.2) and C57BL/6 mice (B.1 and B.2). For each host strain, five infections were initiated with either wild-type parasites (WT) or one of two independently generated *pbmif*-ko lines (KO1 and KO2). In both host strains the densities of circulating reticulocytes were significantly lower in infections initiated with wild-type parasites than in infections initiated with *pbmif*-ko parasites (A.1 and B.1). In contrast, the densities of asexual parasites did not differ significantly in infections initiated with wild-type parasites and infections initiated with *pbmif*-ko parasites (A.2 and B.2).

densities were significantly lower, but only in C57BL/6 mice. Therefore, only reticulocyte parameters differed consistently and significantly between infections with both *pbmif*-ko lines and wild-type infections in BALB/c and C57BL/6 mice (Fig. 7; Tables 1 and 2).

DISCUSSION

It is now clear that the cytokine MIF is an evolutionarily ancient protein with a widespread distribution. MIF homologues in parasitic nematodes have been functionally characterized (21, 49). Furthermore, genome-sequencing projects have shown that MIF homologues are present in the protozoan parasites *Toxoplasma gondii* and *Leishmania major*, but genes encoding MIF are absent from the published genomes of other protozoans, including the related apicomplexan parasites *Cryptosporidium parvum*, *Theileria parvum*, and *Theileria annulata*, and free-living eukaryotes, including *Dictyostelium discoideum* and the ciliate *Tetrahymena thermophila*. Thus, at present the expression of MIF homologues in unicellular eukaryotes is consistently associated with a group of parasitic protozoans that engage in specialized interactions with host cells in blood. Here we describe our initial functional characterization of the *Plasmodium* MIF homologue. The use of the term "homologue" instead of "orthologue" in the case of the parasite-derived MIF is justified, since while we show that there is conservation in function, we cannot at this time rule out additional properties of parasite-derived MIF that are not shared with host MIF.

While *Pb*MIF transcription appears to peak at the trophozoite stage in asexual blood stage parasites, *Pb*MIF is expressed in all parasite forms examined throughout the life cycle and is distributed in the cytoplasm of both the parasite and the infected erythrocyte. These results correlate with *P. falciparum* transcriptome data (5, 32) (PlasmoDB entry PFL1420w). Furthermore, proteome surveys have indicated that the protein is also present in all *P. falciparum* and *P. berghei* life cycle stages analyzed (23, 25). The apparent discrepancy between the presence of the messenger and the presence of the protein might be explained by differences in protein and mRNA stability and turnover. In blood stage parasites, release of *P*MIF is most likely episodic, coinciding with rupture of the infected erythrocytes and release of merozoites. Recombinant His_6-tagged *P*MIF and huMIF elute at apparent molecular masses of 30 and 22 kDa in size exclusion chromatography, and these sizes are both consistent with a dimeric form in solution. Until

recently, the oligomerization state of huMIF had been under debate, with reports showing monomeric, dimeric, and trimeric forms based on cross-linking experiments and dimeric forms based on size exclusion chromatography analyses. A trimeric form in solution was firmly established in sedimentation equilibrium studies (reference 40 and references therein). Since *P*MIF-His_6 appeared to behave like huMIF-His_6 in size exclusion chromatography and huMIF-His_6 appeared to behave like untagged huMIF in previous work (37), the His_6 tag does not appear to affect oligomerization. However, a more in-depth study is required to determine the exact oligomerization status of *P*MIF in solution.

There have been conflicting reports about the relevance of the C terminus of huMIF with regard to enzymatic activity (2, 36). In our assays, a C-terminal His_6 tag did not appear to influence enzymatic activity. Recombinant *P*MIF-His_6 showed tautomerase and oxidoreductase activities, although in both assays the activities were ~20% of the recombinant huMIF-His_6 activities. It is surprising that *P*MIF-His_6 retains oxidoreductase activity in the absence of the second cysteine of the CXXC motif and with the low level of conservation of surrounding sequences. However, given the low level of conservation, we cannot directly compare the *P*MIF and its oxidoreductase activity to the human C60S MIF mutant (which exhibited only background activity compared to wild-type MIF in the HED assay) and its activity. For example, the cysteine in *P*MIF that would correspond to C57 in mammalian MIF is shifted by one register in the alignment (Fig. 1A). Rather, the remaining oxidoreductase activity in *P*MIF can be seen as an intermediate between the activity of human C57S MIF (which exhibits about 60% of the wild-type MIF activity in the HED assay) and the activity of C60S MIF (29). However, we cannot exclude the possibility that the N-terminal cysteine residues may contribute to this effect by transferring protons from reduced glutathione to HED. It is also possible that the structural requirements for oxidoreductase activity are fulfilled in the *P*MIF multimer.

Despite the relatively low enzymatic activity and low sequence similarity compared to huMIF, we found that recombinant *P*MIF-His_6 and the huMIF-His_6 control are equally efficient in reducing AP-1 activation in HEK cells. The exact structural requirements for Jab-1 binding and the inhibition of Jab-1-mediated activation of AP-1 are currently unknown. Previous studies have implied that in huMIF, a structural rearrangement involving the oxidoreductase activity (involving C60) is required for this activity (8, 28, 38). However, peptides spanning the CXXC motif with either the wild-type or C57S/C60S double point mutant sequence can compete for huMIF binding to Jab-1 (27). In the absence of a strong oxidoreductase activity and the crucial C60 residue in *P*MIF, therefore, structural differences may account for *P*MIF's ability to inhibit Jab-1 function. Alternatively, differences in protein uptake or stability in HEK cells between *P*MIF and huMIF might explain this effect.

*P*MIF is not essential for any phase of the *Plasmodium* life cycle. Furthermore deletion of *Pb*MIF did not consistently influence standard virulence parameters, such as red blood cell loss, weight loss, and parasite growth, in the early stages of a *P. berghei* infection. However, infections in two host strains revealed a clear and significant increase in reticulocyte production in the early stages of *pbmif*-ko infection such that the *pbmif*-ko-infected hosts had 1.5- to 4.5-fold more circulating reticulocytes than wild-type-infected hosts. Accurately characterizing the phenotypic effects of MIF expression is difficult using these combinations of *P. berghei* and inbred mice due to the rapid and lethal progression of the infections. Such studies may be more informative if they are carried out with *Plasmodium chabaudi*, which causes a chronic infection in inbred mouse strains. These studies should rely on the *P. chabaudi* genetic transformation technology that has been developed recently (S. Reece and J. Thompson, unpublished data).

None of the studies on the host MIF response to *Plasmodium* infection published thus far have taken the presence of parasite-encoded MIF into account (1, 13, 14, 15, 34, 35). Intriguingly, two of these studies clearly showed that MIF has a role as a host-derived factor inhibiting erythropoiesis in the context of *P. chabaudi* infection in BALB/c mice (34, 35). Our results showing increased reticulocyte numbers in *pbmif*-ko infections match well with these studies and indicate that parasite-encoded MIF might work in concert with host MIF to suppress erythropoiesis in the context of a *Plasmodium* infection. Furthermore, McDevitt et al. observed a mild increase in host survival when infection was carried out with MIF knockout mice. Therefore, it should be of interest to monitor the course of infection of the *pbmif*-ko parasite in a MIF knockout mouse strain. At this time it is unclear how this inhibitory effect on reticulocyte numbers might benefit the parasite; since *P. berghei* is a reticulocyte-preferring parasite, *Pb*MIF appears to act to reduce the preferred host blood cell pool for invasion. However, suppression of erythropoiesis may lead to maintenance of a lower level of parasitemia, which might contribute to a longer-lasting infection. Thus, it is clear that further research on the behavior of the *pmif*-ko parasites in the context of chronic and also genetically diverse infections is required to understand the action of *P*MIF.

Since MIF is a central regulator of the inflammatory response in vertebrates (for a review, see reference 11), release of a parasite homologue is likely to influence this response. It seems counterintuitive that parasites produce a protein that could both initiate a potentially lethal inflammatory immune response and demonstrably reduce the population of red cells preferred for asexual proliferation. However, huMIF has been shown to be able to act upon both pro- and anti-inflammatory pathways, depending on the context and concentration (28; for a review, see reference 11). This raises the intriguing possibility that parasites produce MIF homologues to subversively switch the host immune response from a proinflammatory setting to an anti-inflammatory setting, for instance by expressing an excess amount of parasite MIF that competes with host MIF for effector binding sites and so desensitizes host signaling for the proinflammatory response. Preliminary data indeed show that *P*MIF binds to CD74, which has been identified as a MIF surface receptor (31), with higher affinity than huMIF binds (unpublished observation). We are currently generating a transgenic *P. berghei* parasite which overexpresses *Pb*MIF in the hope that further characterization of the role of *P*MIF in an in vivo setting and further biochemical studies with recombinant *P*MIF will provide additional insights into the role of this cytokine homologue in relation to the host response. Alternatively, parasites may purposefully induce an inflammatory

response, using the host immune system as a means to regulate the population of competing parasites within hosts. Further characterization of host responses to *P*MIF after short-term exposure, as well as long-term exposure, is required to distinguish between these two possibilities. Finally, since parasite MIF homologues are not limited to *Plasmodium*, the findings presented in this study should have implications for the study of host-parasite dynamics in other parasites.

ACKNOWLEDGMENTS

We thank Jai Ramesar for technical assistance with the *P. berghei* transfections and Andrew Read, Rick Maizels, and Judith Allen for critical reading of the manuscript and useful discussions.

This work was supported by grant 072171 from The Wellcome Trust and by grants 812.05.002 and 816.02.001 from The Netherlands Organization for Scientific Research.

REFERENCES

1. **Awandare, G. A., J. B. Hittner, P. G. Kremsner, D. O. Ochiel, C. C. Keller, J. B. Weinberg, I. A. Clark, and D. J. Perkins.** 2006. Decreased circulating macrophage migration inhibitory factor (MIF) protein and blood mononuclear cell MIF transcripts in children with Plasmodium falciparum malaria. Clin. Immunol. **119:**219–225.
2. **Bendrat, K., Y. Al Abed, D. J. Callaway, T. Peng, T. Calandra, C. N. Metz, and R. Bucala.** 1997. Biochemical and mutational investigations of the enzymatic activity of macrophage migration inhibitory factor. Biochemistry **36:**15356–15362.
3. **Bernhagen, J., R. A. Mitchell, T. Calandra, W. Voelter, A. Cerami, and R. Bucala.** 1994. Purification, bioactivity, and secondary structure analysis of mouse and human macrophage migration inhibitory factor (MIF). Biochemistry **33:**14144–14155.
4. **Bloom, B. R., and B. Bennett.** 1966. Mechanism of a reaction in vitro associated with delayed-type hypersensitivity. Science **153:**80–82.
5. **Bozdech, Z., M. Llinas, B. L. Pulliam, E. D. Wong, J. Zhu, and J. L. DeRisi.** 2003. The transcriptome of the intraerythrocytic developmental cycle of Plasmodium falciparum. PLoS Biol. **1:**E5.
6. **Bozza, M., A. R. Satoskar, G. Lin, Lu, B., A. A. Humbles, C. Gerard, and J. R. David.** 1999. Targeted disruption of migration inhibitory factor gene reveals its critical role in sepsis. J. Exp. Med. **189:**341–346.
7. **Breman, J. G.** 2001. The ears of the hippopotamus: manifestations, determinants, and estimates of the malaria burden. Am. J. Trop. Med. Hyg. **64:**1–11.
8. **Burger-Kentischer, A., D. Finkelmeier, M. Thiele, J. Schmucker, G. Geiger, G. E. Tovar, and J. Bernhagen.**. 2005. Binding of JAB1/CSN5 to MIF is mediated by the MPN domain but is independent of the JAMM motif. FEBS Lett. **579:**1693–1701.
9. **Calandra, T., J. Bernhagen, C. N. Metz, L. A. Spiegel, M. Bacher, T. Donnelly, A. Cerami, and R. Bucala.** 1995. MIF as a glucocorticoid-induced modulator of cytokine production. Nature **377:**68–71.
10. **Calandra, T., J. Bernhagen, R. A. Mitchell, and R. Bucala.** 1994. The macrophage is an important and previously unrecognized source of macrophage migration inhibitory factor. J. Exp. Med. **179:**1895–1902.
11. **Calandra, T., and T. Roger.** 2003. Macrophage migration inhibitory factor: a regulator of innate immunity. Nat. Rev. Immunol. **3:**791–800.
12. **Calandra, T., L. A. Spiegel, C. N. Metz, and R. Bucala.** 1998. Macrophage migration inhibitory factor is a critical mediator of the activation of immune cells by exotoxins of Gram-positive bacteria. Proc. Natl. Acad. Sci. USA **95:**11383–11388.
13. **Chaisavaneeyakorn, S., N. Lucchi, C. Abramowsky, C. Othoro, S. C. Chaiyaroj, Y. P. Shi, B. L. Nahlen, D. S. Peterson, J. M. Moore, and V. Udhayakumar.** 2005. Immunohistological characterization of macrophage migration inhibitory factor expression in *Plasmodium falciparum*-infected placentas. Infect. Immun. **73:**3287–3293.
14. **Chaisavaneeyakorn, S., J. M. Moore, C. Othoro, J. Otieno, S. C. Chaiyaroj, Y. P. Shi, B. L. Nahlen, A. A. Lal, and V. Udhayakumar.** 2002. Immunity to placental malaria. IV. Placental malaria is associated with up-regulation of macrophage migration inhibitory factor in intervillous blood. J. Infect. Dis. **186:**1371–1375.
15. **Chaiyaroj, S. C., A. S. Rutta, K. Muenthaisong, P. Watkins, U. M. Na, and S. Looareesuwan.** 2004. Reduced levels of transforming growth factor-beta1, interleukin-12 and increased migration inhibitory factor are associated with severe malaria. Acta Trop. **89:**319–327.
16. **Curfs, J. H., C. C. Hermsen, P. Kremsner, S. Neifer, J. H. Meuwissen, N. Van Rooyen, and W. M. Eling.** 1993. Tumour necrosis factor-alpha and macrophages in Plasmodium berghei-induced cerebral malaria. Parasitology **107:**125–134.
17. **David, J. R.** 1966. Delayed hypersensitivity in vitro: its mediation by cell-free substances formed by lymphoid cell-antigen interaction. Proc. Natl. Acad. Sci. USA **56:**72–77.
18. **de Koning-Ward, T. F., C. J. Janse, and A. P. Waters.** 2000. The development of genetic tools for dissecting the biology of malaria parasites. Annu. Rev. Microbiol. **54:**157–185.
19. **de Kossodo, S., and G. E. Grau.** 1993. Profiles of cytokine production in relation with susceptibility to cerebral malaria. J. Immunol. **151:**4811–4820.
20. **Delahaye, N. F., N. Coltel, D. Puthier, L. Flori, R. Houlgatte, F. A. Iraqi, C. Nguyen, G. E. Grau, and P. Rihet.** 2006. Gene-expression profiling discriminates between cerebral malaria (CM)-susceptible mice and CM-resistant mice. J. Infect. Dis. **193:**312–321.
21. **Falcone, F. H., P. Loke, X. Zang, A. S. MacDonald, R. M. Maizels, and J. E. Allen.** 2001. A Brugia malayi homolog of macrophage migration inhibitory factor reveals an important link between macrophages and eosinophil recruitment during nematode infection. J. Immunol. **167:**5348–5354.
22. **Flieger, O., A. Engling, R. Bucala, H. Lue, W. Nickel, and J. Bernhagen.** 2003. Regulated secretion of macrophage migration inhibitory factor is mediated by a non-classical pathway involving an ABC transporter. FEBS Lett. **551:**78–86.
23. **Florens, L., M. P. Washburn, J. D. Raine, R. M. Anthony, M. Grainger, J. D. Haynes, J. K. Moch, N. Muster, J. B. Sacci, D. L. Tabb, A. A. Witney, D. Wolters, Y. Wu, M. J. Gardner, A. A. Holder, R. E. Sinden, J. R. Yates, and D. J. Carucci.** 2002. A proteomic view of the Plasmodium falciparum life cycle. Nature **419:**520–526.
24. **Gardner, M. J., N. Hall, E. Fung, O. White, M. Berriman, R. W. Hyman, J. M. Carlton, A. Pain, K. E. Nelson, S. Bowman, I. T. Paulsen, K. James, J. A. Eisen, K. Rutherford, S. L. Salzberg, A. Craig, S. Kyes, M. S. Chan, V. Nene, S. J. Shallom, B. Suh, J. Peterson, S. Angiuoli, M. Pertea, J. Allen, J. Selengut, D. Haft, M. W. Mather, A. B. Vaidya, D. M. Martin, A. H. Fairlamb, M. J. Fraunholz, D. S. Roos, S. A. Ralph, G. I. McFadden, L. M. Cummings, G. M. Subramanian, C. Mungall, J. C. Venter, D. J. Carucci, S. L. Hoffman, C. Newbold, R. W. Davis, C. M. Fraser, and B. Barrell.** 2002. Genome sequence of the human malaria parasite Plasmodium falciparum. Nature **419:**498–511.
25. **Hall, N., M. Karras, J. D. Raine, J. M. Carlton, T. W. Kooij, M. Berriman, L. Florens, C. S. Janssen, A. Pain, G. K. Christophides, K. James, K. Rutherford, B. Harris, D. Harris, C. Churcher, M. A. Quail, D. Ormond, J. Doggett, H. E. Trueman, J. Mendoza, S. L. Bidwell, M. A. Rajandream, D. J. Carucci, J. R. Yates III, F. C. Kafatos, C. J. Janse, B. Barrell, C. M. Turner, A. P. Waters, and R. E. Sinden.** 2005. A comprehensive survey of the Plasmodium life cycle by genomic, transcriptomic, and proteomic analyses. Science **307:**82–86.
26. **Haslinger, B., R. Kleemann, K. H. Toet, and T. Kooistra.** 2003. Simvastatin suppresses tissue factor expression and increases fibrinolytic activity in tumor necrosis factor-alpha-activated human peritoneal mesothelial cells. Kidney Int. **63:**2065–2074.
27. **Hoerauf, A., J. Satoguina, M. Saeftel, and S. Specht.** 2005. Immunomodulation by filarial nematodes. Parasite Immunol. **27:**417–429.
28. **Kleemann, R., A. Hausser, G. Geiger, R. Mischke, A. Burger-Kentischer, O. Flieger, F. J. Johannes, T. Roger, T. Calandra, A. Kapurniotu, M. Grell, D. Finkelmeier, H. Brunner, and J. Bernhagen.** 2000. Intracellular action of the cytokine MIF to modulate AP-1 activity and the cell cycle through Jab1. Nature **408:**211–216.
29. **Kleemann, R., A. Kapurniotu, R. W. Frank, A. Gessner, R. Mischke, O. Flieger, S. Juttner, H. Brunner, and J. Bernhagen.** 1998. Disulfide analysis reveals a role for macrophage migration inhibitory factor (MIF) as thiol-protein oxidoreductase. J. Mol. Biol. **280:**85–102.
30. **Kooij, T. W., B. Franke-Fayard, J. Renz, H. Kroeze, M. W. van Dooren, J. Ramesar, K. D. Augustijn, C. J. Janse, and A. P. Waters.** 2005. Plasmodium berghei alpha-tubulin II: a role in both male gamete formation and asexual blood stages. Mol. Biochem. Parasitol. **144:**16–26.
31. **Leng, L., C. N. Metz, Y. Fang, Xu, J., S. Donnelly, J. Baugh, T. Delohery, Y. Chen, R. A. Mitchell, and R. Bucala.** 2003. MIF signal transduction initiated by binding to CD74. J. Exp. Med. **197:**1467–1476.
32. **Le Roch, K. G., Y. Zhou, P. L. Blair, M. Grainger, J. K. Moch, J. D. Haynes, L. De V, A. A. Holder, S. Batalov, D. J. Carucci, and E. A. Winzeler.** 2003. Discovery of gene function by expression profiling of the malaria parasite life cycle. Science **301:**1503–1508.
33. **Lubetsky, J. B., M. Swope, C. Dealwis, P. Blake, and E. Lolis.** 1999. Pro-1 of macrophage migration inhibitory factor functions as a catalytic base in the phenylpyruvate tautomerase activity. Biochemistry **38:**7346–7354.
34. **Martiney, J. A., B. Sherry, C. N. Metz, M. Espinoza, A. S. Ferrer, T. Calandra, H. E. Broxmeyer, and R. Bucala.** 2000. Macrophage migration inhibitory factor release by macrophages after ingestion of *Plasmodium chabaudi*-infected erythrocytes: possible role in the pathogenesis of malarial anemia. Infect. Immun. **68:**2259–2267.
35. **McDevitt, M. A., J. Xie, G. Shanmugasundaram, J. Griffith, A. Liu, C. McDonald, P. Thuma, V. R. Gordeuk, C. N. Metz, R. Mitchell, J. Keefer, J. David, L. Leng, and R. Bucala.** 2006. A critical role for the host mediator macrophage migration inhibitory factor in the pathogenesis of malarial anemia. J. Exp. Med. **203:**1185–1196.
36. **Mischke, R., A. Gessner, A. Kapurniotu, S. Juttner, R. Kleemann, H. Brunner,**

and J. Bernhagen. 1997. Structure activity studies of the cytokine macrophage migration inhibitory factor (MIF) reveal a critical role for its carboxy terminus. FEBS Lett. **414:**226–232.
37. **Mischke, R., R. Kleemann, H. Brunner, and J. Bernhagen.** 1998. Cross-linking and mutational analysis of the oligomerization state of the cytokine macrophage migration inhibitory factor (MIF). FEBS Lett. **427:**85–90.
38. **Nguyen, M. T., J. Beck, H. Lue, H. Funfzig, R. Kleemann, P. Koolwijk, A. Kapurniotu, and J. Bernhagen.** 2003. A 16-residue peptide fragment of macrophage migration inhibitory factor, MIF-(50-65), exhibits redox activity and has MIF-like biological functions. J. Biol. Chem. **278:**33654–33671.
39. **Pastrana, D. V., N. Raghavan, P. FitzGerald, S. W. Eisinger, C. Metz, R. Bucala, R. P. Schleimer, C. Bickel, and A. L. Scott.** 1998. Filarial nematode parasites secrete a homologue of the human cytokine macrophage migration inhibitory factor. Infect. Immun. **66:**5955–5963.
40. **Philo, J. S., T. H. Yang, and M. LaBarre.** 2004. Re-examining the oligomerization state of macrophage migration inhibitory factor (MIF) in solution. Biophys. Chem. **108:**77–87.
41. **Reininger, L., O. Billker, R. Tewari, A. Mukhopadhyay, C. Fennell, D. Dorin-Semblat, C. Doerig, D. Goldring, L. Harmse, L. Ranford-Cartwright, J. Packer, and C. Doerig.** 2005. A NIMA-related protein kinase is essential for completion of the sexual cycle of malaria parasites. J. Biol. Chem. **280:**31957–31964.
42. **Rodriguez-Sosa, M., L. E. Rosas, J. R. David, R. Bojalil, A. R. Satoskar, and L. I. Terrazas.** 2003. Macrophage migration inhibitory factor plays a critical role in mediating protection against the helminth parasite *Taenia crassiceps*. Infect. Immun. **71:**1247–1254.
43. **Rosengren, E., R. Bucala, P. Aman, L. Jacobsson, G. Odh, C. N. Metz, and H. Rorsman.** 1996. The immunoregulatory mediator macrophage migration inhibitory factor (MIF) catalyzes a tautomerization reaction. Mol. Med. **2:**143–149.
44. **Satoskar, A. R., M. Bozza, S. M. Rodriguez, G. Lin, and J. R. David.** 2001. Migration-inhibitory factor gene-deficient mice are susceptible to cutaneous *Leishmania major* infection. Infect. Immun. **69:**906–911.
45. **Swope, M., H. W. Sun, P. R. Blake, and E. Lolis.** 1998. Direct link between cytokine activity and a catalytic site for macrophage migration inhibitory factor. EMBO J. **17:**3534–3541.
46. **van Dijk, M. R., C. J. Janse, J. Thompson, A. P. Waters, J. A. Braks, H. J. Dodemont, H. G. Stunnenberg, G. J. van Gemert, R. W. Sauerwein, and W. Eling.** 2001. A central role for P48/45 in malaria parasite male gamete fertility. Cell **104:**153–164.
47. **Waters, A. P., A. W. Thomas, M. R. van Dijk, and C. J. Janse.** 1997. Transfection of malaria parasites. Methods **13:**134–147.
48. **Wu, Z., T. Boonmars, I. Nagano, T. Nakada, and Y. Takahashi.** 2003. Molecular expression and characterization of a homologue of host cytokine macrophage migration inhibitory factor from Trichinella spp. J. Parasitol. **89:**507–515.
49. **Zang, X., P. Taylor, J. M. Wang, D. J. Meyer, A. L. Scott, M. D. Walkinshaw, and R. M. Maizels.** 2002. Homologues of human macrophage migration inhibitory factor from a parasitic nematode. Gene cloning, protein activity, and crystal structure. J. Biol. Chem. **277:**44261–44267.

Editor: J. F. Urban, Jr.